Proceedings of BS2013:
13th Conference of International Building Performance Simulation Association, Chambéry, France, August 26-28

INVERSE METHOD FOR FLOW RECONSTRUCTION USING GAS TRACERS IN BUILDING ENVIRONMENTS

William César[1,3], Alexandre Nassiopoulos[2], and Frédéric Bourquin[1]
[1]Université Paris-Est, IFSTTAR, CoSys, Marne-la-Vallée, France
[2]LUNAM Université, IFSTTAR, CoSys, Bouguenais, France
[3]Université Paris-Est, ESIEE-Paris, Noisy-le-Grand, France

ABSTRACT

Air quality monitoring as well as comfort or overall energy performance require accurate information on airflow patterns, while they are particularly difficult to assess in existing buildings. We present an innovative instrumentation system using gas tracers, based on the combined use of several highly sensitive emerging micro-gas chromatographs (μGC) as pollutant sensors and an identification method for data processing. The strategy used is based on the optimal control theory in which only the time evolution of the components of the velocity field needs to be reconstructed thanks to the use of a proper orthogonal decomposition (POD) method. We present numerical results showing evidence of the performance of the approach in the case of a unimodal flow.

INTRODUCTION

Airflow patterns are very difficult to assess in existing buildings. However, they are of uttermost importance for the overall energy performance and for indoor air quality monitoring. In order to limit energy losses, building envelopes tend to be more and more insulated and actual air change rates (ACR) are reduced. As a consequence it has been observed that pollutant levels can be higher inside than outside while we spend about 90% of our time indoor (EPA, 2001). Insufficient ventilation is responsible for unhealthy indoor conditions to the point that a new term was invented to name this preoccupying phenomenon: the *sick building syndrom*. A more careful design and control of ventilation are necessary in order to satisfy both requirements on energy saving and air quality, as well as occupant comfort. This in turn raises the need for airflows assessment and monitoring techniques. Therefore, accurate quantification and documentation on building airflows are essential.

In this scope, many techniques have been developed. Among them, direct measurement methods consist in directly measuring the air velocity at given points through the use of sensors such as hot wire anemometers (Mueller and Vogel, 1994). With this technique, it is however difficult to efficiently measure a flow in all directions with sufficient sensitivity. In addition, indirect methods using gas tracers are more popular as they allow getting more information on the building, such as leak detection or air change rate (Laussmann and Helm, 2011) that is essential, for instance, to the assessment of air quality under conditions of natural ventilation. In the previous studies, sensors were often either very limited in terms of performance or unaffordable in view of real-life deployment. For instance, optical units such as photoacoustic spectrometers (Harren and G. Cotti, 2000) were popular for their accuracy but these devices were expensive and bulky. Passive samplers based on carbon adsorbent are also widely used for their low cost and simplicity (Shinohara et al., 2010), but this technique has a low time resolution and does not allow real-time monitoring.

Nevertheless, ongoing miniaturization and integration of sensor technologies enable one to consider instrumentation systems based on several sensor units spread over the building. Micro-gas chromatographs are sensors amongst the best candidates to be used in such application. These microsystems, in the manner of their popular (but bulky) laboratory counterparts, are based on the principle of gas separation: a gas sample is injected in a *capillary column* in which analytes travel at different speeds before being detected downstream. An additional functional unit called *preconcentrator* can be used to accumulate the analytes for a certain period of time before rapidly releasing them in the column, which greatly amplifies the detection signal to the price of a longer analysis time. This modularity makes micro-chromatographs highly sensitive and selective devices. Many efforts are being made in order to improve the capabilities of each individual μGC component. As a small set of examples, one can cite nanotube-coated separation column (Reid et al., 2009), fast-response optical sensors (Reddy et al., 2011) or preconcentrators optimized for pollution monitoring (Camara et al., 2011)). Other groups demonstrated the possibility of using particular injection techniques to further improve sensitivity of such systems (Cesar et al., 2013). Using a hybrid micro-gas chromatograph, detection capabilities of down to ppt levels (which is extremely low) with a measurement time of few minutes have been reported (Chang et al., 2010). Real-time analysis of air in contaminated homes using two μGC prototypes

have also been perfomed (Kim et al., 2011). In this latter study, more than 45 volatile organic compounds (VOC) could be separated in less than one minute. In fact, μGC systems have the potential of being able to detect very small quantities of very large kinds of common gases (they are particularly adapted to the detection of VOCs), including the usable tracer gas recommended by the ASTM (Standard E741), with a time resolution of the order of a minute. Last but not least, monolithic integration of micro-chromatography systems, including pumping and injection units, would give them the great advantage of being small-sized and batch-fabricated, so that they could be easily spread within a room.

In this study, we present an innovative instrumentation system, based on the combined use of several micro-gas chromatographs, gas tracer and an inverse identification method for data processing. This paper focuses on the numerical treatment of the data. For the sake of simplicity, we consider a source emitting a single gas, although a multi-tracer technique could be used with the type of sensors we consider. We use a strategy based on the optimal control theory, which consists in identifying the velocity field that minimizes the misfit between data provided by sensors and the direct model output. This model is based on the isothermal Navier-Stokes (NS) and advection-diffusion equations, which are coupled together because of the advection process. Minimization is performed by solving a gradient-based descent algorithm where the regularized cost functional gradient is derived by solving an adjoint problem. The spatial velocity field is projected on a finite dimensional space using POD model reduction. Only the time evolution of the components of the velocity field in the reduced space needs to be reconstructed. This assumption dramatically reduces the computational cost. The reliability of a similar approach, in the case of a multizone model, was demonstrated by (L. Chen, 2012) where an orthonormal basis was obtained through the use of singular value decomposition (SVD). Our test case is a room with two apertures that allow air circulation. Direct and adjoint problems are solved using finite element method (FEM). We present numerical results showing evidence of the performance of the approach in the case of a unimodal flow.

DESCRIPTION OF THE PROBLEM

Test case

For this study, we chose a test case inspired from the ADN-bati benchmark case (CNRS/Limsi,Univ. Réunion/PIMENT, INES/LOCIE) which consists of a 6.5m-long and 2.5m-high room including two apertures allowing cross-ventilation. We use a 2D representation of the room, in a vertical cross section as depicted in figure (1). The velocity flow is driven by prescribing a parabolic distribution on the left window.

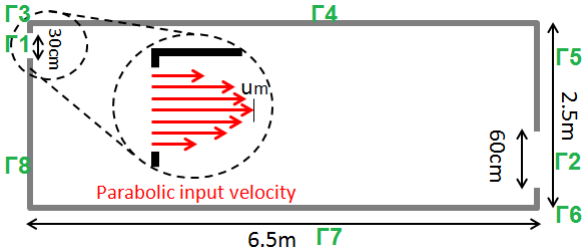

FIGURE *1 – Geometry used for simulations and spatial distribution of input velocity*

Mass transfer equation

The concentration evolution of the gas tracer in the room can be described by the following parabolic equation :

$$\begin{cases} \dfrac{\partial c}{\partial t} + (\vec{u}.\vec{\nabla})c - D\triangle c = s & \Omega \times [0,T] \\ \vec{\nabla}c.\vec{n} = 0 & \partial\Omega \\ c(x,0) = c_0(x) & \Omega \end{cases} \quad (1)$$

In this advection-diffusion equation, c is the concentration (ppm), $\vec{u}$ is the velocity field ($m.s^{-1}$), D is the diffusion coefficient ($m^2.s^{-1}$) and $s(x,t)$ is a source term ($ppm.s^{-1}$). $x \in \Omega$ and $t \in [0,T]$ are the space and time variables respectively. $\vec{n}$ is a vector normal to the boundary $\partial\Omega$.

Flow characteristics

Although the airflow is the unknown control parameter that we aim at reconstructing, we know that it obeys the rules of fluid dynamics. In a building under isothermal conditions, the following incompressible Navier-Stokes (NS) equations apply :

$$\begin{cases} \dfrac{\partial \vec{u}}{\partial t} + (\vec{u}.\vec{\nabla})\vec{u} - \nu\triangle\vec{u} + \dfrac{1}{\rho_0}\vec{\nabla}P = \vec{f} & \Omega \times [0,T] \\ \vec{\nabla}.\vec{u} = 0 & \Omega \\ \vec{u} = \vec{y_i} & \Gamma_i \subset \partial\Omega \end{cases} \quad (2)$$

In equation (2), ν is the kinematic viscosity of air ($m^2.s^{-1}$), ρ_0 is its density ($kg.m^{-3}$), P is the pressure (bar) and $\vec{f}$ represents the gravity forces ($m.s^{-2}$). The flow is assured by defining the velocity at the left aperture according to a normal parabolic spatial distribution (1) and the velocity on the right window can then be deduced from the incompressibility property. In addition, the no-slip boundary condition ($\vec{y_i} = 0$) is set on the walls ($i \in [\![3,8]\!]$).

Inverse problem

To reconstruct the flow, we use local information on concentration evolution from the N sensors that are placed within the room at positions $\{x_k\}_{k=1}^N$. Note that although they are capable of measuring multiple gas concentrations, we assume that we use a single tracer gas so that we get data as N functions of time $\boldsymbol{c}^d = \{c_k^d(t)\}_{k=1}^N$. We also make use of the direct physical models that describe the whole evolution of

concentration (equation (1)) assuming that all system parameters, including the velocity field, are known.
The identification method we present is based on the optimal control theory. It consists in seeking the velocity field that minimizes the misfit between the direct model response and the data given by the sensors. This kind of problem have been extensively studied in the literature, for instance in the fields of heat transfer (Liu et al., 2012) or atmospheric sciences (Pudykiewicz, 1998).
In the case we use a POD basis $\vec{\boldsymbol{\xi}}$ of size M for flow projection, the velocity field writes :

$$\vec{u}(x,t) \simeq u_0(x) + \sum_{i=1}^{M} a_i(t)\vec{\xi}_i(x) \tag{3}$$

and as a consequence, the problem boils down to identifying the set of time functions $\boldsymbol{a} = \{a_i(t)\}_{i=1}^{M}$.
The difference between the data and the direct model output is measured through the cost functional :

$$J(\boldsymbol{a}) = \frac{1}{2}\left\|\boldsymbol{\mathcal{C}}(c(x,t;\boldsymbol{a})) - \boldsymbol{c^d}\right\|_{\mathcal{M}}^2 + \frac{\epsilon}{2}\left\|\boldsymbol{a}\right\|_{\mathcal{U}}^2 \tag{4}$$

In this equation, $\mathcal{M} = L^2([0,T])^N$ and $\mathcal{U} = L^2([0,T])^M$ are the measure and control spaces respectively endowed with the following scalar products $\|u\|_{\mathcal{M}}^2 = (u,u)_{\mathcal{M}}$ and $\|u\|_{\mathcal{M}}^2 = (u,u)_{\mathcal{M}}$ with

$$(\boldsymbol{u},\boldsymbol{v})_{\mathcal{M}} = \sum_{k=1}^{N}\int_0^T u_k v_k\, dt \tag{5}$$

$$(\boldsymbol{u},\boldsymbol{v})_{\mathcal{U}} = \sum_{i=1}^{M}\int_0^T u_i v_i\, dt \tag{6}$$

Here $\boldsymbol{\mathcal{C}}$ is an observation operator that maps the direct model's output to the observations in $\mathcal{M}$. We will choose $\boldsymbol{\mathcal{C}}$ such that :

$$\begin{cases} u \in \mathcal{V} = L^2(\Omega\times[0,T]), \mathbf{v} \in \mathcal{M} \\ \mathbf{v}(t) = \boldsymbol{\mathcal{C}}(u(x,t)) = \displaystyle\int_\Omega u(x,t)\boldsymbol{\psi}(x)dx \end{cases} \tag{7}$$

In practice, the functions $\boldsymbol{\psi} = \{\psi_k\}_{k=1}^{M}$ are unitary sharp gaussian functions modeling local measurement of each sensor.

$$\psi_k(x) = \alpha_k \exp(-\frac{(x-x_k)^2}{2{d_k}^2}) \tag{8}$$

α_k is a unitary-scaling coefficient and d_k is the mean measurement distance of the k^{th} sensor. The choice of the observation operator must fit as well as possible the sensor's mode of operation. Here we consider the case of an ideal sensor whose output is a measurement of the concentration at a precise time. Microchromatographs can also perform an averaging of the concentration over a certain period of time when they are used with a preconcentrator. In this case, an other observation operator should be defined and that could be the subject of an other study. The term $\frac{\epsilon}{2}||\boldsymbol{a}||_{\mathcal{U}}^2$ (ϵ is a small positive coefficient) in equation (4) is a Thikonov regularization term that is added in order to avoid the ill-posedness of such control problem (Franklin, 1974).
Finally, the identification problem consists in finding the unknown set of parameters $\boldsymbol{a} \in \mathcal{U}$ that minimizes the functionnal J :

$$J(\boldsymbol{a}) = \inf_{\boldsymbol{b}\in\mathcal{U}} J(\boldsymbol{b}) \tag{9}$$

The resolution of this problem can be performed through a *descent method* which consists in iteratively computing parameters that tend towards the point where the gradient ∇J vanishes. The method for computing this cost functional as well as the descent algorithm will be presented below.

IDENTIFICATION METHOD

Flow projection: method of snapshots

Let us consider a spatial orthonormal basis $\vec{\boldsymbol{\xi}}$ such that $\vec{\boldsymbol{\xi}} = \{\vec{\xi}_i(x)\}_{i=1}^{\infty}$, and let be $\vec{u}_0(x)$ the time-averaged flow. By projecting $\vec{u} - \vec{u}_0(x)$ into this basis, it comes :

$$\vec{u}(x,t) = u_0(x) + \sum_{i=1}^{\infty} a_i(t)\vec{\xi}_i(x) \tag{10}$$

As a consequence, instead of seeking $\vec{u}$ in the whole space $\Omega\times[0,T]$, it is possible to reconstruct the flow by determining the collection of time functions $\boldsymbol{a} = \{a_i(t)\}_{i=1}^{\infty}$. In practice, the size of the projection basis is limited to M elements, and this order reduction introduces errors in the identification process. However, it is possible to efficiently reduce this error by choosing a basis whose vectors support most of the flow energy. Such basis can be found using the *a priori* information known from the NS equations. As a matter of fact, it is often possible to limit the size to a rather low value of M, which dramatically reduces the computational cost. This technique, called POD is extensively employed in CFD since its first report (Lumley, 1967), and is also used in pattern recognition (Sirovich and Kirby, 1987) and in various simulations (Sempey et al., 2009) and control (Li et al., 2012) problems. Different types of POD methods are presented in (Luchtenburg et al., 2009). The method we use is the "method of snapshots", which consists in constructing the basis $\vec{\boldsymbol{\xi}}$ from a set of M steady velocity fields taken from a simulation based on equation (2) at different times $t_i \in [0,T]$:

$$\vec{u}_i = \vec{u}(x,t_i), \quad i \in [\![1,M]\!] \tag{11}$$

A mean fluctuation value is computed :

$$\vec{u}_0 = \frac{1}{M}\sum_{i=1}^{M}\vec{u}_i(x) \tag{12}$$

and the so-called *correlation matrix* $\boldsymbol{C}$ is derived.

$$\boldsymbol{C}_{ij} = \frac{1}{M}\int_\Omega (\vec{u}_i - \vec{u}_0).(\vec{u}_j - \vec{u}_0)dx \tag{13}$$

$\boldsymbol{C}$ is Hermitian since it is real and symmetric. It is therefore diagonalizable and its eigenvalues $\{\lambda_i\}_{i=1}^M$ are positive. The eigenvector $\boldsymbol{a}^{[i]} = (a_1^{[i]}, ..., a_M^{[i]})$ verify the equation :

$$\boldsymbol{C}\boldsymbol{a}^{[i]} = \lambda_i \boldsymbol{a}^{[i]} \tag{14}$$

Before using the eigenvectors in the POD basis computation, the eigenvectors coefficients are scaled so that :

$$\boldsymbol{a}^{[i]}.\boldsymbol{a}^{[j]} = M\lambda_i \delta_{ij} \tag{15}$$

The POD modes $\{\vec{\xi}_i\}_{i=1}^M$ are finally computed as follows :

$$\vec{\xi}_i = \frac{1}{M\lambda_i} \sum_{m=1}^{M} a_m^{[i]} (\vec{u}_m - \vec{u}_0) \tag{16}$$

The energy contained in each mode is directly given by the associated eigenvalue, so that it is easy to sort the modes by importance and to truncate the basis as needed.

The method of snapshots is a particular case of POD in which the decomposition is performed in the time domain. Inversion models based on this method are then limited to reconstructing one particular unsteady flow with well known parameters. In a more general case, one or several flow parameters such as velocity boundary conditions may vary and the resulting flow may not be properly described in the chosen basis. In order to avoid that issue, the POD decomposition must be performed both in time and parameters domains, which leads to a more exhaustive basis, adapted to in-situ analysis.

Optimization algorithm

The direct problem (equation (1)) is non-linear with respect to the sought parameters $\boldsymbol{a}$. As a consequence, the optimization problem described in the previous paragraph is not linear and the cost functional is not quadratic. We will use the *Levenberg-Marquardt* descent algorithm that can be used to solve this particular kind of problems. This method consists in successively minimizing a cost functional built around successive linearization points of equation (1). Each of these functionals is minimized with the *conjugate gradient method with optimal descent step*, that requires the computation of their gradient. This gradient is derived from the solution of an *adjoint problem* that have a structure similar to the direct problem of equation (1).

The first order linearization of the model equation (1) around the linearization point $\boldsymbol{a}^i$ is given in equation (17). It is obtained by considering a small variation of the unknown parameters $\delta\boldsymbol{a}$ around $\boldsymbol{a}^i$.

$$c(\boldsymbol{a}^i + \delta\boldsymbol{a}) \simeq c(\boldsymbol{a}^i) + \delta c(\delta\boldsymbol{a}) \tag{17}$$

We introduce the new functional $J_i'(\delta\boldsymbol{a})$ built using this linearized problem (17) :

$$\begin{aligned} J_i'(\delta\boldsymbol{a}) = \quad & \frac{1}{2}\| \int_\Omega (c(\boldsymbol{a}^i) + \delta c)\boldsymbol{\psi}\, dx - \boldsymbol{c^d}\|_{\mathcal{M}}^2 \\ & + \frac{\epsilon}{2}\|\delta\boldsymbol{a}\|_{\mathcal{U}}^2 \end{aligned} \tag{18}$$

The term δc is the solution of the linearized first order sensitivity equation (19), derived from the linearization of equation (1) around $\boldsymbol{a}^i$ in the case where the velocity field $\vec{u}$ is projected as in equation (3).

$$\begin{cases} \dfrac{\partial \delta c}{\partial t} + (\vec{u}_0 + \sum_{n=1}^{M} a_n^i \vec{\xi}_n).\vec{\nabla}\delta c - D\triangle\delta c = \\ \qquad -(\sum_{n=1}^{M} \delta a_n^i \vec{\xi}_n.\vec{\nabla}) c(\boldsymbol{a}^i) & \Omega\times[0,T] \\ D\vec{\nabla}\delta c.\vec{n} = 0 & \partial\Omega \\ \delta c(x,0) = 0 & \Omega \end{cases} \tag{19}$$

In the above *sensitivity equation*, the control parameters $\{\delta a_n^i\}_{n=1}^M$ appear in a source term and are linear with respect to δc. Since J_i' is quadratic, standard linear minimization processes such as conjugate gradient method can be used in this case.

The descent algorithm consists in finding at step i the unknown parameter $\boldsymbol{a}^{i+1}$ such that :

$$J_i'(\boldsymbol{a}^{i+1} - \boldsymbol{a}^i) = \inf_{\boldsymbol{a}\in\mathcal{U}} J_i'(\boldsymbol{a} - \boldsymbol{a}^i) \tag{20}$$

At each iteration, a new linearization point $\boldsymbol{a}^{i+1}$ is then computed in the descent direction of the functionnal J. Each of these minimization processes being itself iterative, the optimization algorithm includes two nested loops. Besides, the gradient of J_i' that indicates the descent direction is computed using the well-known adjoint method (Yamaleev et al., 2010) (D.N. Srinath, 2010), which consists in deriving $\nabla J_i'$ from the adjoint problem of equation (19) :

$$\begin{cases} -\dfrac{\partial p}{\partial t} - (\vec{u}_0 + \sum_{n=1}^{M} a_n^i \vec{\xi}_n).\vec{\nabla} p - D\triangle p = \\ \quad \sum_{k=1}^{N} \left(\int_\Omega (c(\boldsymbol{a}^i) + \delta c)\psi_k dx - c_k^d \right) \psi_k & \Omega\times[0,T] \\ (D\vec{\nabla}p + (\vec{u}_0 + \sum_{n=1}^{M} a_n^i \vec{\xi}_n)p).\vec{n} = 0 & \partial\Omega \\ p(x,T) = 0 & \Omega \end{cases} \tag{21}$$

Note that this adjoint equation has a similar structure with the direct equation (19), where time is reversed and where the source term includes the data misfit. However, the final condition $p(x,T) = 0$ has a consequence on the reconstructed parameters. As a matter of fact, the gradient and consequently the descent direction at $t = T$ will always be equal to zero, so that the final boundary value of the reconstructed parameters will be equal to the arbitrary initial guess. This problem can be avoided using particular functional spaces as presented in (Bourquin and Nassiopoulos, 2011).

The gradient of J_i' is obtained as a function of the *adjoint state* p, $c(\boldsymbol{a}^i)$ and $\delta\boldsymbol{a}$:

$$\boldsymbol{\nabla} J_i'(\delta\boldsymbol{a}) = \int_\Omega -p\vec{\nabla}c(\boldsymbol{a}^i).\vec{\boldsymbol{\xi}} dx + \epsilon\delta\boldsymbol{a} \tag{22}$$

This expression is obtained from operations on the variational form of (19), equation (21) and the expression of the cost functional (18). These rather cumbersome but standard computations are not presented in this document for the sake of clarity but as an example similar computations can be found in (Nassiopoulos and Bourquin, 2013).
As a summary, the Levenberg-Marquardt algorithm writes :

- Initialization : $i = 0$, $\boldsymbol{a}^0$
- i-loop
  - Initialization : $j = 0$, $\delta\boldsymbol{a}_i^0$
  - Compute $c^i = c(\boldsymbol{a}^i)$ satisfying (1)
  - j-loop
    1. Compute $\delta c_i^j = \delta c(\delta \boldsymbol{a}_i^j)$ satisfying (19)
    2. Compute p_i^j then $\boldsymbol{\nabla} J_i'^j$ from (21) and (22)
    3. Compute the descent direction for j ≥ 1

$$\boldsymbol{d}^j = \boldsymbol{\nabla} J_i'^j + \frac{\|\boldsymbol{\nabla} J_i'^j\|_{\mathcal{U}}^2}{\|\boldsymbol{\nabla} J_i'^{j-1}\|_{\mathcal{U}}^2}\boldsymbol{d}^{j-1} \qquad (23)$$

    4. Compute the optimal descent step

$$\rho^j = \frac{(\boldsymbol{\nabla} J_i'^j, \boldsymbol{d}^j)_{\mathcal{U}}}{(A\boldsymbol{d}^j, \boldsymbol{d}^j)_{\mathcal{U}}} \qquad (24)$$

    5. Set $\delta\boldsymbol{a}_i^{j+1} = \delta\boldsymbol{a}_i^j - \rho^j \boldsymbol{d}^j$
    6. Increment j and break the j-loop if $j = J$
  - Set $\boldsymbol{a}^{i+1} = \boldsymbol{a}^i + \delta\boldsymbol{a}_i^J$
  - Increment i and break the i-loop if $i = I$
- The optimal solution is finally $\boldsymbol{a}^I$

The steps 3 and 4 are the realizations of the conjugate gradient with optimal step method, in which A is an operator based on equations (19), (21) and (22). This method was first introduced in (Hestenes and Stiefel, 1952).

SIMULATION RESULTS

The different problems have been solved using the finite element method. Domain meshing, problem resolution as well as matrix diagonalization were performed with the open-source software environment FreeFEM++.

POD basis construction

In this section, we will present an example of POD basis construction using the method of snapshots.
First, the unsteady Navier-Stokes equation (2) is solved using a regular triangle mesh with 10000 nodes. We take a 3-node linear (P1) elements for the pressure and 6-node quadratic (P2) elements for the velocity. We use an implicit formulation of the problem, and the non-linear advective term is comprehended using the method of characteristics as described in (Hecht and Pironneau, 2012). The simulation is run with a time interval $T = 10min$ and a timestep of $dt = 1s$, and the maximum flow velocity imposed at the left window is $u_m = 0.05m.s^{-1}$. In our example, we choose the set of 40 snapshots that corresponds to the solutions taken at times $\{t_i = 10i\ s\}_{i=0}^{39}$. Note that these snapshots correspond to the transient flow when the air starts to be blown from the left to the right window and crosses the room. Besides, the resulting basis will have a maximal size of 39.

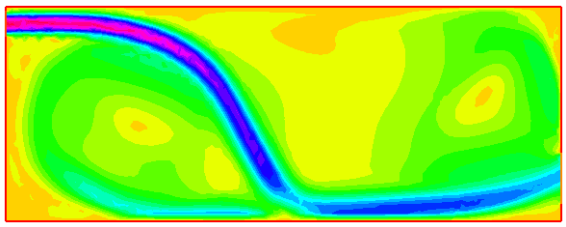

FIGURE 2 – *Euclidian norm of the velocity snapshot taken at $t = 6min$. Scale : 0 to $0.05m.s^{-1}$*

The mean field $\vec{u}_0$ and the basis vectors are then computed as explained before.

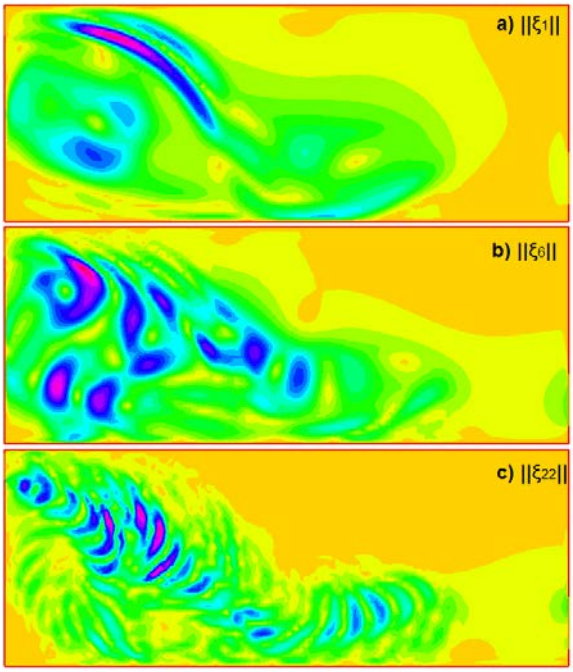

FIGURE 3 – *Euclidian norm of modes 1 ($\vec{\xi}_1$), mode 6 ($\vec{\xi}_6$) and 22 ($\vec{\xi}_{22}$) of the orthonormal POD basis*

The relative amount of energy E_i carried by the i^{th} mode is :

$$E_i = \frac{\lambda_i}{\sum_{j=1}^{M}\lambda_j} \qquad (25)$$

The rapid decrease of the eigenvalues and the convergence of their sum implies that the energy E_i is almost equal to the real energy of the flow if M is large enough. The values E_i as well as the corresponding eigenvalues λ_i for each 6 first modes are reported in table (1). The orthogonality property between each mode is verified through the use of the scalar product :

$$(\vec{\xi}_i, \vec{\xi}_j) = \int_\Omega \vec{\xi}_i.\vec{\xi}_j dx = \delta_{ij} \qquad (26)$$

TABLE *1 – Eigenvalue and relative energy carried by the 6 first modes of the POD basis*

Mode i	Eigenvalue λ_i	Relative energy E_i
1	$4.22\ 10^{-6}$	22.1%
2	$3.22\ 10^{-6}$	16.9%
3	$2.42\ 10^{-6}$	12.7%
4	$1.83\ 10^{-6}$	9.6%
5	$1.51\ 10^{-6}$	7.9%
6	$1.20\ 10^{-6}$	6.3%

On can notice that almost 80% of the energy is carried by 15% of the modes.

Inversion method: case of a unidimensional basis

We will present in this part the performance of the inversion method considering a single mode. The problem thus reduces to the case where the pattern of the flow is known but its time evolution is not. The working principle of the algorithm should easily extend to the multi-mode case, *i.e.* to the case where the flow pattern is unknown.

In this problem, we consider that $\vec{u}_0 = \vec{0}$ and $\dim \boldsymbol{a} = 1$ so that $\vec{u} = a_1(t)\vec{\xi}_1(x)$. We take as a realistic basis $\vec{\xi}_1(x)$ the normalized steady state solution of the Stokes problem, which is equivalent to the problem of equation (2) without the advective term. The direct and adjoint models used in the optimization algorithm are discretized in space using linear ($P1$) elements and simulations are run over a time period of $T = 30min$, and sensor measurements are performed every $dt = 1min$. This value is taken large in order to fit the micro-chromatograph typical measurement time. We take the characteristic of a standard COV such as methane, that a micro-chromatograph is able to detect. The gas diffusivity is set to $D = 5\ 10^-3m^2.s^{-1}$.

The source term is a narrow gaussian function placed in front of the left window that also has a gaussian time evolution :

$$s(x,t) = \sigma \exp\left(-\frac{(x-x_s)^2+(y-y_s)^2}{2{d_s}^2} - \frac{(t-t_s)^2}{2{t_{sd}}^2}\right) \quad (27)$$

with

TABLE *2 – Parameters of the source function* $s(x,t)$

Parameter	Unit	Value
σ	$ppm.s^{-1}$	10
x_s	m	0.5
y_s	m	2.2
d_s	m	0.25
t_s	s	150
y_{sd}	s	90

Sensor optimal placement and quantity could be the subject of a whole study. In our example, we will simply use two sets of 3 (set 1) and 6 (set 2) sensors, placed as shown in figure (4).

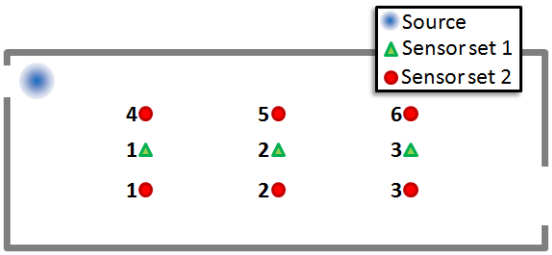

FIGURE *4 – Placement of the source and sensors*

To test the algorithm, data is simulated by running a direct mass transfer simulation (equation (1)) with known velocity field and parameters. The corresponding concentration field is then processed using the measurement operator (equation (7)) to obtain the simulated data for each sensor. The arbitrarily chosen velocity field temporal evolution is a time-centered gaussian function :

$$a_1(t) = \alpha \exp\left(-\frac{(t-t_c)^2}{2{t_d}^2}\right) \quad (28)$$

where we take $\alpha = 0.05m.s^{-1}$, $t_c = 15min$ and $t_d = 5min$. This function will be the target function that the algorithm will try to reconstruct. The simulated data obtained with this velocity evolution is shown on figure (5) and figure (6) for the sensors sets 1 and 2 respectively.

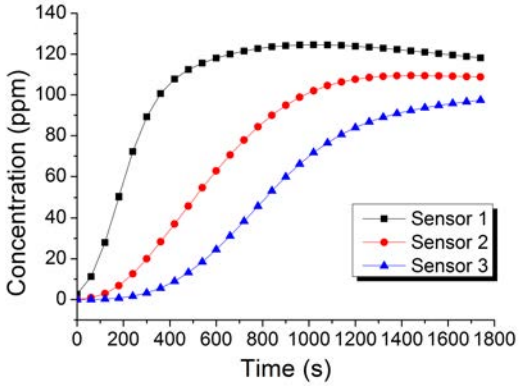

FIGURE *5 – Data recorded by sensor set 1*

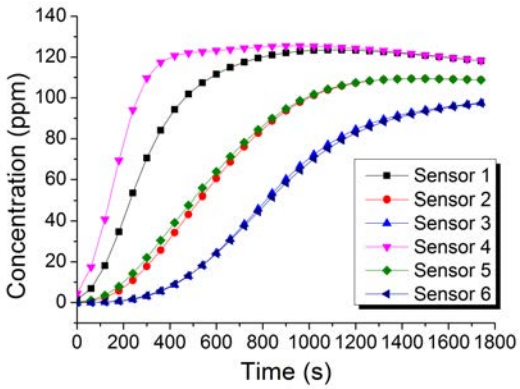

FIGURE *6 – Data recorded by sensor set 2*

We take $I = 5$ and $J = 5$ as loop break-parameters, as good results were obtained with these values. The

total number of iterations is thus 25. Figure (7) shows the evolution of each functional $J_i'^j$ over the algorithm iterations. One can notice that although every $J_i'^j$ is decreasing, the functional value may increase after a new i-loop iteration. However, the overall functional tends to decrease as expected. Besides, the functional for sensor set 2 is higher than for sensor set 1, as more information is recorded by its 3 extra sensors.

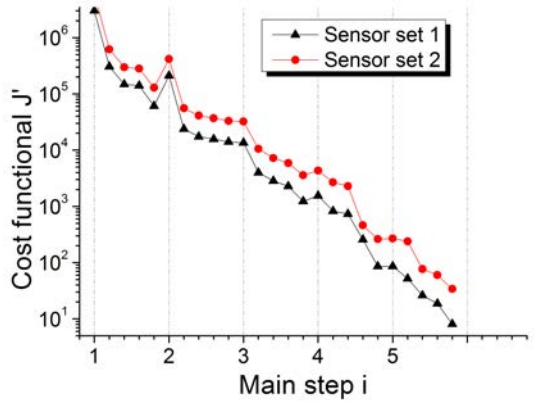

FIGURE 7 – *Cost functional evolution through iterations in both i and j loops and for both sensors sets*

In figure (8), one can see the different values of the reconstructed velocity profile over the i-loop iterations, for sensor set 1. From the first iteration, the gaussian-shape is already roughly approximized, and at step 4, the target and the reconstructed curve almost overlap.

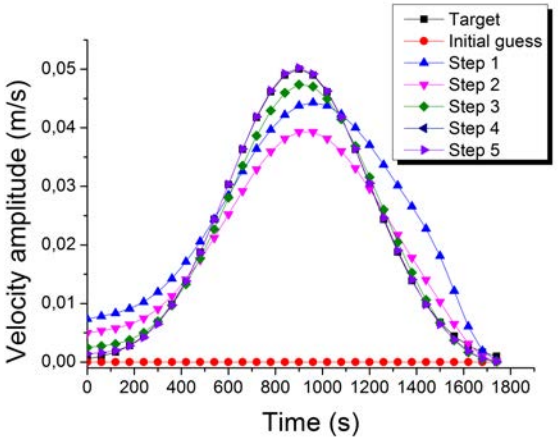

FIGURE 8 – *Reconstruced velocity profiles through iterations in the i-loop, for sensor set 1*

The precision of the reconstruction at step i can be evaluated through the relative reconstruction error, that is given by :

$$\epsilon_a^i = \left(\frac{\int_0^T (a_1 - a_r^i)^2 dt}{\int_0^T {a_1}^2 dt} \right)^{1/2} \quad (29)$$

where a_r^i denotes the reconstructed velocity profile at step i. Likewise, an relative error can be computed for the concentration c :

$$\epsilon_c^i = \left(\frac{\int_\Omega \int_0^T (c(a_1) - c_(a_r^i)^2 dx dt}{\int_\Omega \int_0^T c(a_1)^2 dx dt} \right)^{1/2} \quad (30)$$

where c is computed from equation (1). Figure (9) shows these errors as a function of the step in i-loop. One can notice that the number of sensors does not impact much on the result in this test case. The error is even higher with the set of 6 sensors. This reveals the importance of sensor placement which is a main parameter to optimize the performances. Besides, the relative error on the concentration is always lower than the error on the velocity. This is due to the fact that the algorithm tends to decrease the data misfit in terms of concentration, and not in terms of velocity.
Finally, the concentration error after five iterations is lower than 0.3%, while the airflow is reconstructed with an error lower than 2.9%.

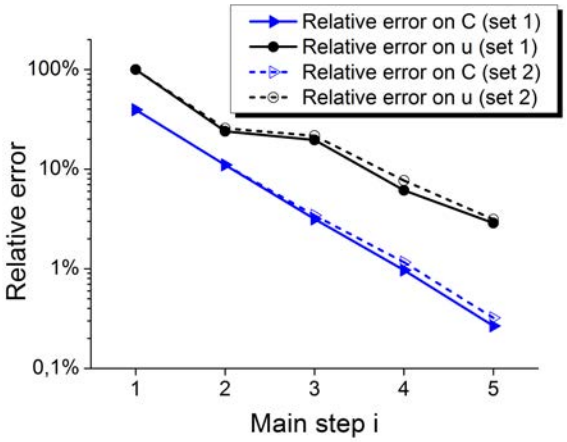

FIGURE 9 – *Reconstruction error on the concentration ϵ_c^i and the velocity ϵ_a^i through iterations in the i-loop*

CONCLUSION

In this paper, we propose an instrumentation system for airflow characterization, based on the combined use of several micro gas chromatographs, gas tracer and an inverse identification method for data processing. We describe an inversion method based on the optimal control theory where the spatial velocity field is reconstructed in a finite dimensional space obtained through the use of a partial orthogonal decomposition method. Simulation results that demonstrate the performance of the method are presented in the case of a unimodal POD basis. Demonstration of the method using a higher order basis will be presented in a future work. This method should find valuable utilizations in the fields of building diagnosis and control, for applications such as indoor air quality analysis as well as ventilation strategies for energy efficiency and thermal comfort.

NOTATIONS

Bold parameters such as $\boldsymbol{d}$ are multi-element parameters. Arrowed parameters such as $\vec{u}$ are spatial vectors.

REFERENCES

Bourquin, F. and Nassiopoulos, A. 2011. Inverse reconstruction of initial and boundary conditions of a heat transfer problem with accurate final state. *International Journal of Heat and Mass Transfer*, 54 :3749–3760.

Camara, E., Breuil, P., Briand, D., de Rooij, N., and Pijolat, C. 2011. A micro gas preconcentrator with improved performance for pollution monitoring and explosives detection. *Analytica Chimica Acta*, 688(2) :175–182.

Cesar, W., Flourens, F., Kaiser, C., Sutour, C., and Angelescu, D. 2013. High-sensitivity micro-gas chromatography using stocastic injection techniques. *Proc. IEEE MEMS2013*, pages 997–1000.

Chang, H., Kim, S., Sukaew, T., Bohrer, F., and Zellers, E. 2010. Microfabricated gas chromatograph for sub-ppb determinations of tce in vapor intrusion investigations. *Proc. Eurosensors XXIV*, 5 :973–976.

D.N. Srinath, S. M. 2010. An adjoint method for shape optimization in unsteady viscous flows. *Journal of Computational Physics*, 229(6) :1994–2008.

EPA 2001. Healthy building, healthy people : a vision for the 21st century. *United State Environmental Protection Agency publication*.

Franklin, J. 1974. On thikhonov's method for ill-posed problems. *Mathematics of computation*, 28(128) :889–907.

Harren, J. and G. Cotti, J. O. S. L. H. 2000. Photoacoustic spectroscopy in trace gas monitoring. *Encyclopedia of Analytical Chemistry*, pages 2203–2226.

Hecht, F. and Pironneau, O. 2012. *FreeFEM++ manual*.

Hestenes, M. R. and Stiefel, E. 1952. Methods of conjugate gradients for solving linear systems. *Journal of Research of the National Bureau of Standards*, 49(6) :409–436.

Kim, S., Bryant, J., Chang, H., and Zellers, E. 2011. Field testing of a microgc propotype : real time analysis of a tce vapors in indoor air in contaminated homes. *Proc. Risk Science Symposium*.

L. Chen, J. W. 2012. Inverse estimation of indoor airflow patterns using singular value decomposition. *Applied Mathematical Modelling*, 36(6) :2627–2641.

Laussmann, D. and Helm, D. 2011. *Air change measurements using tracer gases*. InTech.

Li, K., Su, H., Chu, J., and Xu, C. 2012. A fast-pod model for simulation and control of indoor thermal environment of buildings. *Bulding and Environment*.

Liu, D., Zhao, F., Wang, H., Rank, E., and Kou, G. 2012. Inverse determination of building heating profiles from the knowledge of measurements within the turbulent slot-vented enclosure. *Internal journal of heat and mass transfer*, 55 :4596–4612.

Luchtenburg, D., Noack, B. R., and Schlegel, M. 2009. An introduction to the pod galerkin method for fluid flows. Technical report, Berlin Institute of Technology.

Lumley, J. 1967. The structure of inhomogeneous turbulent flows. *Atmos. Turb. and Radio Wave Prop.*, pages 166–178.

Mueller, H. and Vogel, P. 1994. Methods for investigating indoor air conditions of ventilated rooms. *AIVC Conference proceedings*, 1 :101–108.

Nassiopoulos, A. and Bourquin, F. 2013. On-site building walls characterization. *Numerical Heat Transfer, Part A : Applications*, 63(3) :179–200.

Pudykiewicz, J. 1998. Application of adjoint tracer trahsnport equations for evaluating source parameters. *Atmospheric environment*, 32(17) :3039–3050.

Reddy, K., Guo, Y., Liu, J., Lee, W., Oo, M., and Fan, X. 2011. On-chip fabry-pérot interferometric sensors for micro-gas chromatography detection. *Sensors and Actuators B : Chemical*, 159(1) :60–65.

Reid, W., Stadermann, M., Bakajin, O., and Synovec, R. 2009. High-speed, temperature programmable gas chromatography utilizing a microfabricated chip with an improved carbon nanotube stationary phase. *Talanta*, 77 :1420–1425.

Sempey, A., Inard, C., Ghiaus, C., and Allery, C. 2009. Fast simulation of temperature distribution in air conditionned rooms by using proper orthogonal decomposition. *Building and Environment*, 44 :280–289.

Shinohara, N., Kataoka, T., Takamine, K., Butsugan, M., Nishikima, H., and Gamo, M. 2010. Modifier perfluorocarbon tracer method for measuring effective multizone exchange rates. *J. Environ. Res. Public Health*, pages 3348–3358.

Sirovich, L. and Kirby, M. 1987. Low-dimensional procedure for the characterization of human faces. *J. Optical Society of America*, 4 :519–524.

Yamaleev, N., Diskin, B., and Nielsen, E. 2010. Local-in-time adjoint-based method for design optimization of unsteady flows. *Journal of computational physics*, 229(14) :5394–5407.